JOURNAL OF COMPUTATIONAL PHYSICS 19, 77–89 (1975)

Numerical Solution of the Vlasov Equation with the Accurate Space Derivative Method

JENÖ GAZDAG

IBM Corporation, Palo Alto Scientific Center, Palo Alto, California 94304

Received November 13, 1974; revised April 18, 1975

A numerical procedure is described for the solution of the Vlasov–Poisson system of equations in two and three phase-space variables. In this approach the distribution function is represented over a computational mesh. Time integration is done by advancing the distribution in real phase space as in finite difference methods. However, the derivatives with respect to all the phase-space variables are computed by finite Fourier transform methods. Truncation errors are principally due to time discretization, and are controlled by the choice of the time step. As for the phase-space variables, the accuracy of the computation is determined by the harmonic content of the distribution function, since contributions due to coupling between Fourier modes are computed with high accuracy. The numerical method has been tested on linear and nonlinear problems, and our results agree remarkably well with those obtained from the Fourier–Hermite method. However, for comparable overall accuracy, the present method is about ten times more efficient (CPU time) than the Fourier–Hermite method in some of the examples discussed in this paper.

I. INTRODUCTION

It has been found that the Accurate Space Derivative (ASD) method is well suited to the numerical solution of certain time-dependent partial differential equations [1–6]. In this numerical approach the functions are represented over some computational grid. The integration with respect to the time t is based on a Taylor series in t. Expressions containing space derivative-terms are then substituted for the time derivatives. The accurate computation of these space derivative terms is done effectively by the use of finite Fourier transform techniques. This approach to computing the space derivative terms results in numerical schemes which are substantially more accurate than existing finite difference methods [7].

In this paper we describe a method of numerical solution for the Vlasov–Poisson system of equations based on the ASD principle. We consider a scheme of third order in time for a problem with one spatial dimension and two velocity dimensions. We demonstrate the feasibility and accuracy of our numerical method

through numerical experiments related to linear and nonlinear Landau damping. These results are compared with those obtained by the Fourier–Hermite method [8, 9]. To test the numerical scheme for a computer plasma with an externally applied constant magnetic field, we study stable longitudinal electron waves propagating perpendicularly to the magnetic field [10, 11]. Sharp peaks in the frequency spectrum define the frequencies of these oscillations [12, 13]. These frequencies compare well with those obtained from the linear theory for small amplitude waves.

II. The Nonlinear Vlasov Equation

The system of equations under consideration consists of the Vlasov equation for the electron distribution $f(x, v_x, v_y, t)$ [14]

$$\frac{\partial f}{\partial t} + v_x \frac{\partial f}{\partial x} - E \frac{\partial f}{\partial v_x} - \omega_c \left(v_y \frac{\partial f}{\partial v_x} - v_x \frac{\partial f}{\partial v_y} \right) = 0, \tag{1}$$

and the Poisson equation for the electric field E,

$$\frac{\partial E}{\partial x} = 1 - \int f \, dv_x \, dv_y . \tag{2}$$

These equations are written in dimensionless units. The basic units of time t and velocity v are the reciprocal of the plasma frequency $(\omega_p)^{-1}$ and the mean thermal velocity v_t, respectively. Length x is measured in units of the Debye length. The cyclotron frequency ω_c is specified in units of ω_p.

For computing purposes the distribution function f can be represented conveniently either in a rectangular or in a cylindrical coordinate system. We have programmed Eqs. (1) and (2) in both coordinate systems following essentially the same numerical method in each. For the rectangular case the computational domain R was set to be

$$R = \{(x, v_x, v_y) | \, 0 \leqslant x < x_0 , \, | v_x | \leqslant v_c , \, | v_y | \leqslant v_c \}. \tag{3}$$

In the cylindrical coordinate system the computational domain was defined as

$$C = \{(x, v, \phi) \mid 0 \leqslant x < x_0 , \, | v | \leqslant v_c , \, 0 \leqslant \phi < 2\pi \}, \tag{4}$$

where

$$v = (v_x^2 + v_y^2)^{1/2} \tag{5}$$

and

$$\phi = \tan^{-1}(v_y / v_x). \tag{6}$$

The free-streaming ($E = 0$) solution of Eq. (1) corresponds to a uniform rotation of $f(x, v_x, v_y)$ in the $(v_x - v_y)$ plane and a displacement along x. Consequently, the cylindrical coordinate system has some advantages over the rectangular one. If a rectangular mesh were used to represent the $(v_x - v_y)$ plane, the mesh points outside the largest circle that could be inscribed in the rectangle would be wasted. The representation of f by a cylindrical mesh also results in stability conditions more favorable than those of a rectangular mesh.

In this paper we shall consider solution methods developed for the cylindrical coordinate system. The Vlasov equation expressed in terms of the phase-space variables x, v, and ϕ reads

$$\frac{\partial f}{\partial t} + v \cos \phi \frac{\partial f}{\partial x} - E\left(\cos \phi \frac{\partial f}{\partial v} - \frac{\sin \phi}{v} \frac{\partial f}{\partial \phi}\right) + \omega_c \frac{\partial f}{\partial \phi} = 0, \tag{7}$$

and the Poisson equation for the electric field E takes the form

$$\frac{\partial E}{\partial x} = 1 - \int f v \, dv \, d\phi. \tag{8}$$

The velocity plane is represented by the computational mesh shown in Fig. 1.

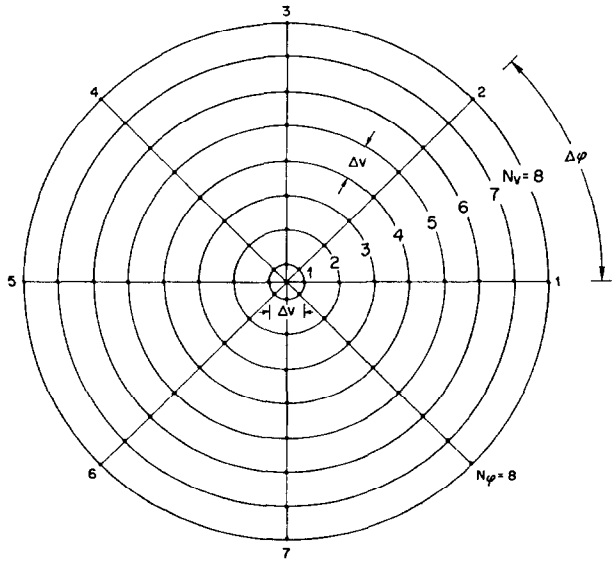

FIG. 1. Computational mesh for the velocity plane.

No mesh point was placed at the origin since this would have inconvenienced the computation of the term

$$E(\sin \phi/v)(\partial f/\partial \phi)$$

in Eq. (7). Instead, the mesh was designed such that the smallest velocity associated with any mesh point is $\Delta v/2$.

III. The Numerical Method

The numerical approach to be described here is based on the principles of the ASD method [1]. The electron distribution is advanced by approximating $f(x, v, \phi, t + \Delta t)$ from $f(x, v, \phi, t)$ by means of the expression

$$f(x, v, \phi, t + \Delta t) = \sum_{l=0}^{p} \frac{\partial^l f(x, v, \phi, t)}{\partial t^l} \frac{(\Delta t)^l}{l!}, \tag{9}$$

where p is the order of the method. We shall only be concerned with third-order schemes, i.e., $p = 3$. The time derivatives in Eq. (9) are obtained from Eq. (7) by successive differentiation:

$$\frac{\partial f}{\partial t} = -v \cos \phi \frac{\partial f}{\partial x} + E\left(\cos \phi \frac{\partial f}{\partial v} - \frac{\sin \phi}{v} \frac{\partial f}{\partial \phi}\right) - \omega_c \frac{\partial f}{\partial \phi} = 0, \tag{10}$$

$$\frac{\partial^2 f}{\partial t^2} = -v \cos \phi \frac{\partial}{\partial x} \frac{\partial f}{\partial t} + E\left(\cos \phi \frac{\partial}{\partial v} \frac{\partial f}{\partial t} - \frac{\sin \phi}{v} \frac{\partial}{\partial \phi} \frac{\partial f}{\partial t}\right) - \omega_c \frac{\partial}{\partial \phi} \frac{\partial f}{\partial t} + \frac{\partial E}{\partial t}\left(\cos \phi \frac{\partial f}{\partial v} - \frac{\sin \phi}{v} \frac{\partial f}{\partial \phi}\right), \tag{11}$$

$$\frac{\partial^3 f}{\partial t^3} = -v \cos \phi \frac{\partial}{\partial x} \frac{\partial^2 f}{\partial t^2} + E\left(\cos \phi \frac{\partial}{\partial v} \frac{\partial^2 f}{\partial t^2} - \frac{\sin \phi}{v} \frac{\partial}{\partial \phi} \frac{\partial^2 f}{\partial t^2}\right) + 2 \frac{\partial E}{\partial t}\left(\cos \phi \frac{\partial}{\partial v} \frac{\partial f}{\partial t} - \frac{\sin \phi}{v} \frac{\partial}{\partial \phi} \frac{\partial f}{\partial t}\right) + \frac{\partial^2 E}{\partial t^2}\left(\cos \phi \frac{\partial f}{\partial v} - \frac{\sin \phi}{v} \frac{\partial f}{\partial \phi}\right) - \omega_c \frac{\partial}{\partial \phi} \frac{\partial^2 f}{\partial t^2}. \tag{12}$$

The derivatives with respect to the phase-space variables x, v, and ϕ are computed by using finite Fourier transform methods [1]. For example, let $F(k, v, \phi, t)$ be the finite Fourier transform of $f(x, v, \phi, t)$ with respect to the variable x. Then the partial derivative of f with respect to x is given by

$$\frac{\partial f}{\partial x} = \sum_k ikF(k, v, \phi, t) \exp(ikx), \tag{13}$$

where $i = (-1)^{1/2}$ and the summation in Eq. (13) is carried out for all wavenumbers k which can be represented over the computational mesh without ambiguity. This method of computing space derivatives gives results which are substantially more accurate than those obtained from finite difference approximations.

Partial derivatives with respect to ϕ are computed without any difficulty because of the natural periodicity in this variable. The calculation of the derivatives with respect to v is slightly more involved. In order to assure continuity through the origin (see Fig. 1), the Fourier transformation is carried out over $2N_v$ mesh points covering a velocity range of $2v_c$. This is done by concatenating samples corresponding to any ϕ value with those whose angle is $\phi + \pi$.

The electric field E and its time derivatives $\partial E/\partial t$ and $\partial^2 E/\partial t^2$ in Eqs. (10)–(12) are computed by standard Poisson solver techniques from f and its time derivatives $\partial f/\partial t$ and $\partial^2 f/\partial t^2$ by the equations

$$\frac{\partial}{\partial x}\left(\frac{\partial^l E}{\partial t^l}\right) = 1 - \int \frac{\partial^l f}{\partial t^l}\, v\, dv\, d\phi; \qquad l = 0, 1, 2. \tag{14}$$

IV. Accuracy and Stability

Accuracy and stability criteria for a numerical method are often estimated by studying test cases which are simplified versions of physical problems which the numerical scheme is intended to study. Typically, truncation errors are established from linear tests and are expressed in terms of the wavenumber, the value of a uniform velocity field, and the time step of computation. Such linear analysis of stability and accuracy of the ASD convective schemes was described elsewhere [1]. The results of such analysis can also be applied to estimating the errors in complex nonlinear cases providing certain conditions are satisfied. These conditions require that: (1) the space derivatives of f in Eqs. (9)–(12) be computed with high accuracy; and (2) the aliasing errors be negligible. The first condition is satisfied by the ASD method since the space differencing errors are negligibly small. The second condition stipulates that errors resulting from the truncation of the spatial frequency domain be negligible. This is equivalent to saying that all frequency components (in phase space) of the distribution function can be represented on the computational mesh without ambiguity. When this requirement is seriously violated, the computation breaks down [7, 15].

The magnitude of aliasing errors depends upon the relationship between the frequency spectrum of the true solution and the highest frequency which can be supported by the computational mesh. The effect of truncation in frequency space is almost independent of the numerical method used. For example, the "recurrence of the initial state" in plasma computations, which is an aliasing phenomenon,

manifests itself in the same qualitative manner in different numerical methods [7, 15, 17], including the present one. Therefore, aliasing effects will be ignored when the accuracy of the numerical method is considered.

Under these assumptions, significant computational errors are due to time discretization only. We shall make the simplifying assumption that the time dependence of $f(x, v, \phi, t)$ at any point of the phase space is $\exp(i\omega t)$, where ω may be real or complex, and

$$\omega = \omega(x, v, \phi) \tag{15}$$

in the most general case. The time derivatives of f can then be expressed as

$$\partial^l f/\partial t^l = (i\omega)^l f, \tag{16}$$

and Eq. (9) becomes

$$f(x, v, \phi, t + \Delta t) = \sum_{l=0}^{p} (i\omega)^l \frac{(\Delta t)^l}{l!} f(x, v, \phi, t). \tag{17}$$

Since the exact solution corresponding to Eq. (17) is $f(x, v, \phi, t)\exp(i\omega\,\Delta t)$ it is apparent that the truncation error is

$$\epsilon = \left[\exp(i\omega\,\Delta t) - \sum_{l=0}^{p} (i)^l \frac{(\omega\,\Delta t)^l}{l!}\right] f. \tag{18}$$

By considering cases in which ω is real, the error in Eq. (18) can be expressed conveniently as amplitude error and phase error as defined in [1]. The magnitudes of these error terms are shown in [1, Figs. 1, 2] as functions of the true phase $\omega\,\Delta t$.

Stability conditions for a Cartesian coordinate system are described in [1]. This linear stability criterion specifies an upper limit ($\sim 0.547\,\pi$ for the third order method) for the change in phase angle of any Fourier component in one time step. In other words, the total phase change (the sum over all phase-space variables), for any Fourier modes which can be represented over the mesh, must be less than $\sim 0.547\,\pi$. In order to apply the result of the linear stability analysis, which assumes a uniform velocity field, to a practical situation, we use the maxima of v and E over C (Eq. (4)), denoted by v_m and E_m, respectively. Similarly, we let k_m, l_m, and m_m be the highest frequencies (wavenumbers) with respect to the variables x, v, and ϕ. The corresponding phase change will not exceed $v_m k_m\,\Delta t$, $E_m l_m \cos\phi\,\Delta t$, and $[(E_m \sin\phi)/v + \omega_c]\, m_m\,\Delta t$ along x, v, and ϕ, respectively. Substituting $\phi = 0$ in these expressions and letting v assume its smallest value, $\Delta v/2$ (see Fig. 1), we obtain the following requirement for stability.

$$[v_m k_m + E_m(l_m + (2m_m/\Delta v)] + \omega_c m_m]\,\Delta t \leqslant 0.547\,\pi. \tag{19}$$

The values of k_m, l_m, and m_m are $\pi/\Delta x$, $\pi/\Delta v$, and $\pi/\Delta\phi$, respectively.

V. Numerical Results

The numerical examples described below are intended to demonstrate the accuracy and efficiency of the ASD method. We first consider examples for unmagnetized plasma, i.e., $\omega_c = 0$. In this case the three phase-space variables can be reduced to two since we are only interested in the $\phi = 0, \pi$ line of Fig. 1. Eqs. (7) and (8) become

$$(\partial f/\partial t) + v(\partial f/\partial x) - E(\partial f/\partial v) = 0 \tag{20}$$

and

$$\frac{\partial E}{\partial x} = 1 - \int f\, dv. \tag{21}$$

The equilibrium distribution is chosen to be Maxwellian, i.e.,

$$f_0(v) = (2\pi)^{-1/2} \exp(-\tfrac{1}{2}v^2), \tag{22}$$

and the initial condition for the electron distribution is set as

$$f(x, v, 0) = f_0(v)(1 + \alpha \cos kx), \tag{23}$$

where k is the wavenumber and α is the initial perturbation amplitude. The initial electric field is

$$E_0 = \alpha/k, \tag{24}$$

and the bounce frequency ω_B is given by [8]:

$$\omega_B = (\alpha)^{1/2}. \tag{25}$$

In what follows we shall use N_x, N_v, and N_ϕ to designate the number of mesh points used along the variables x, v, and ϕ (see Fig. 1), respectively. Note that N_v refers to the velocity domain $0 < v \leqslant v_c$, therefore N_ϕ is no less than 2.

In the first example we test the time reversibility of the numerical solutions. Here we used $N_x = 8$, $N_v = 128$, and $N_\phi = 2$, with $v_c = 5$. With $k = 0.5$ and $\alpha = 0.001$ the distribution is integrated forward 1000 time steps ($50\omega_p^{-1}$). At this point the sign of Δt is set negative and the distribution is integrated backward. The oscillation frequency and damping rate obtained from the numerical output averaged over the peaks from $t = 4.7$ to $t = 26.9$ are $\omega = 1.417$ and $-\gamma = 0.1537$, respectively. The exact values obtained from Landau's dispersion equation are $\omega = 1.416$ and $-\gamma = 0.1534$. The time behavior of the first Fourier mode of the electric field E is shown in Fig. 2. The damping process reverses at $t = 50$ when Δt becomes negative and plotting continues in the positive t direction. At $t = 100$, E is less than its initial ($t = 0$) value by 0.2%. This amount of amplitude error (damping)

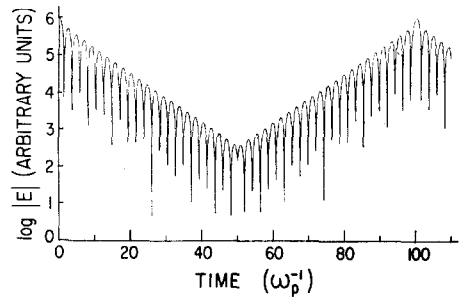

FIG. 2. Electric field versus time for $k = 0.5$ with $\alpha = 0.001$. The sign of Δt is changed at $t = 50$, causing a reversal of the integration. Plotting continues in the positive t direction.

is expected from the time differencing alone. We can see this if we calculate the error by the expression of Eq. (18). For small values of $\omega\,\Delta t$ the contribution of the $l = 4$ term would be to correct the amplitude error of the third order method. This can be seen by inspecting [1, Figs. 1, 2]. In our case, $\omega = 1.417$ and $\Delta t = 0.05$ for which the $l = 4$ term in (18), i.e., $(\omega\,\Delta t)^4/4!$, is $\sim 10^{-6}$, which is approximately the amplitude error per time step. In 2000 Δt this amplitude error should accumulate to 0.2%, as we obtain at $t = 1000$ in the example shown in Fig. 2.

Figure 3 shows the time evolution of the first three Fourier modes for $\alpha = 0.1$. We used $N_x = 16$ which allows the correct representation of at least seven spatial harmonics. For the velocity domain we used $N_v = 128$ and $N_\phi = 2$ with $v_c = 5$.

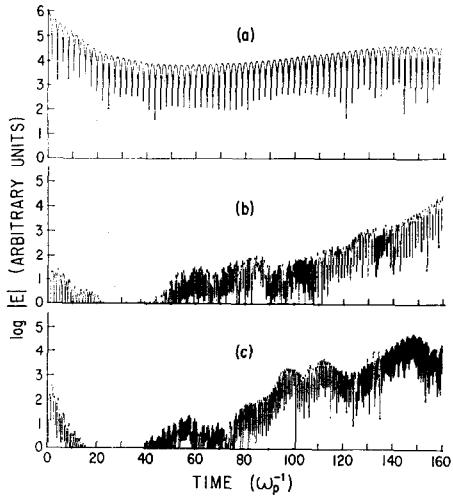

FIG. 3. Electric field versus time for $\alpha = 0.1$. (a) Main wave, $k_1 = 0.5$; (b) second Fourier mode, $k_2 = 1$; (c) third Fourier mode, $k_3 = 1.5$.

This permits an alias-free computation of the main wave for about 160 time units; the recurrence of the initial state would occur at $2\pi/k\,\Delta v \cong 320$. In order to obtain quantitative error estimates in this example, we compared the main wave amplitude with that obtained with the Fourier–Hermite method. In the latter method the distribution function is expanded in Fourier series in space and Hermite polynomials in velocity. This reduces the Vlasov equation to a set of first order ordinary differential equations. An excellent review of this method is given by Armstrong *et al.* [9]. The time for which one can study approximately collisionless phenomena is $t = M^{1/2}/k$, where M is the number of Hermite polynomials employed. A velocity resolution corresponding to the $N_v = 128$ case would require 6400 Hermite terms.

The peak values of E obtained by these two methods agree up to three significant figures for $t \leqslant 35$. The main wave amplitude shows a minimum at about $t = 56.$, the same as reported [8] by the Fourier–Hermite method. Following this minimum, the main wave grows, and it attains a peak at about $t \cong 145$. The second and third Fourier harmonics undergo a short period of damping followed by consistent growth. Both of these modes attain an amplitude of the same order of magnitude as that of the main wave around $t = 140$ to 160.

The effect of a strong nonlinear perturbation, $\alpha = 0.5$, is shown in Fig. 4 for $k = 0.5$. The computational mesh was the same as in the previous case. The main wave damps much more rapidly than expected from the Landau theory. It has a

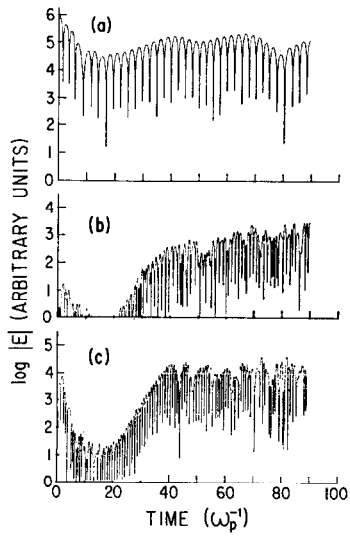

FIG. 4. Electric field versus time for $\alpha = 0.5$. (a) Main wave, $k_1 = 0.5$; (b) second Fourier mode, $k_2 = 1$; (c) third Fourier mode, $k_3 = 1.5$.

minimum at $t \sim 15.4$, which agrees well with numerical results obtained with finite difference methods [8]. The first mode reaches its maximum at $t \sim 41$, which is nearly the same as shown in [8, Fig. 9]. Nührenberg [16] obtained this peak value before $t = 39$, whereas Knorr's results [17, Fig. 3] show no evidence of such a maximum for $t \leqslant 50$. The second and third modes show a strong growth between $t = 20$ and 40. The third mode is saturated at $t \sim 40$ while the second mode still shows a mild growth for $t = 40$ to 90. The behavior of the second and third modes shown in Fig. 4 agrees qualitatively with Nührenberg's results [16] although in the present case the oscillations of the third mode show more regularity for $t = 20$ to 40.

The time evolution of the main wave shown in Fig. 4 is not in complete agreement with the one obtained by finite difference methods [8, Fig. 9]. In the present results the second minimum ($t = 51$) and the second maximum ($t = 67$) of the electric field occur sooner, and have higher values than in the finite difference result. Furthermore, the second maximum at $t = 67$ is somewhat higher than the first one at $t = 41$. This is contrary to the finite difference results whose behavior is in better qualitative agreement with theoretical predictions [18, p. 69], according to which the amplitude of the main wave shows damped oscillatory modulation [18, Fig. 4.4]. Since the truncation errors in finite difference methods are orders of magnitude larger than those in the ASD method, the most probable source of computational error would be due to inadequate grid resolution or roundoff. In order to establish whether these results were affected by such errors, we repeated the computations of the $\alpha = 0.5$ case with various grid sizes ($N_x = 8$, 16; $N_v = 128$, 256; and $N_\phi = 2$) using double precision arithmetic.

We found that even with $N_x = 8$, by setting to zero the highest spatial Fourier mode, $k_4 = 2$, of the distribution function at each time step, the behavior of the main wave was similar to that shown in Fig. 4, which was computed with $N_x = 16$. We performed another set of tests using $N_x = 16$, $N_v = 128$, and $N_\phi = 2$, in which one, three and five of the highest spatial Fourier coefficients of the distribution function were set to zero in each time step. The amplitude of the main wave varied only a few percent between these cases. However, the second maximum near $t = 67$ was at least 10 % higher than the first in all cases. This indicates that there were no appreciable aliasing effects with respect to the x variable.

We found that the velocity resolution of the grid with $N_v = 128$ gridpoints over $0 \leqslant v \leqslant 5$ was also adequate. When we halved Δv by using $N_v = 256$, we found that the amplitude of the main wave agreed with the $N_v = 128$ case within 1 % for $t < 80$.

The above results give strong evidence that the main wave shown in Fig. 4 is not affected appreciably by aliasing or numerical recurrence phenomena. What they indicate is that, in the strong nonlinear case, the modulating envelope of the electric field is not always a smoothly damped oscillatory function as predicted by

the theoretical model based on electron trapping. This model assumes that trapped electrons execute oscillatory motion in the potential well of the wave, and that the bulk of the electrons move together in some orderly fashion. The result is a very smooth uniform modulating envelope as shown in Fig. 3a for $\alpha = 0.1$. In the $\alpha = 0.5$ case, however, the initial wave energy is 25 times greater than for $\alpha = 0.1$. Consequently, the electrons responsible for the energy exchange experience stronger accelerations and cannot maintain such orderly oscillations in the potential well as in weaker nonlinear cases. As a matter of fact, the theoretical model [18] was not intended to predict plasma behavior for the $\alpha = 0.5$ case, which could hardly be realized in a physical experiment. The reason for the surprisingly smooth and physically appealing behavior of the electric field obtained with finite difference computations can be attributed to the intrinsic dissipation and dispersion with respect to both x and v variables in that method.

In order to test the ASD method for magnetized plasma, a Maxwellian equilibrium electron distribution

$$f_0(v) = (2\pi)^{-1} \exp(-\tfrac{1}{2}v^2) \tag{26}$$

was chosen, and the intial condition was set to be

$$f(x, v, \phi, 0) = f_0(v)(1 + \alpha \cos kx), \tag{27}$$

where k is the wavenumber of the longest wave. The perturbation amplitude was set as $\alpha = 0.001$.

The time behavior of the electric field amplitude is characterized by steady, undamped oscillations. These oscillations are not monochromatic, because of the presence of several modes, so that the E vs time plots are not very informative. The sequence of the first Fourier coefficients of E over 4096 time steps was Fourier transformed with respect to t. An example of the so-obtained spectrum is shown in Fig. 5. The locations of the peaks correspond to frequencies of the Bernstein modes for waves propagating perpendicularly to the magnetic field [10, 11]. Computer simulation by means of particle models of such Cyclotron Harmonic Waves has been reported [12, 13]. In both cases the results were the fluctuation spectra of the computer plasma. In the present case, however, the waves are the result of the initial conditions (27) with no significant amount of noise present. The positions of the peak values in Fig. 5 agree with those predicted by small amplitude perturbation theory [10, 11] within 1 %.

The computations were carried out on an IBM System 360/Mod 195 computer. The results presented here were obtained by using simple precision arithmetic. Double precision was also used to test against roundoff error. The speed of computation is nearly the same in both single and double precision on this computing system. The nonlinear examples shown in Fig. 3 and 4, using 4098 grid points

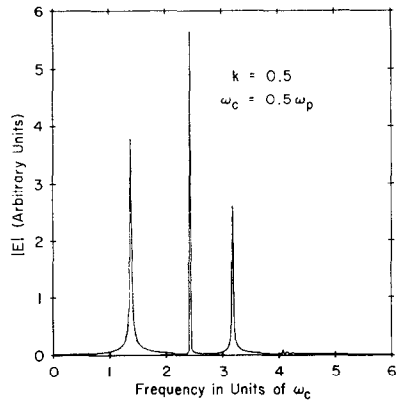

FIG. 5. Spectrum of electrostatic oscillations in a magnetized plasma.

($N_x = 16$, $N_v = 128$, and $N_\phi = 2$) required 0.39 sec of computation (CPU time) per time step. For example, the $\alpha = 0.1$ case shown in Fig. 3 required, with $\Delta t = 0.05$, approximately 21 min of CPU time.

VI. CONCLUSIONS

We have described a numerical procedure, based on the ASD method, for the solution of the Vlasov–Poisson system of equations in two and three phase-space variables. The time integration of the distribution function is performed in real phase-space as in the case of ordinary finite difference methods. However, the derivatives with respect to the phase-space variables are computed by Fourier methods. As a result, phase-space derivatives are accurate within the limit to which a function can be defined over a finite set of mesh points. Hence, truncation errors are small and can be controlled by the choice of the time step Δt.

We have given some examples to demonstrate the precision of this numerical method. From the linear Landau damping example with time reversal at $t = 50$, we have seen that space differencing errors are practically nonexistent, i.e., no significant amount of information is lost in the process of computing the partial derivatives with respect to phase-space variables. It has been shown that the 0.2% error in the initial amplitude after 100 time units (2000 Δt) is roughly the same as one expects due to time differencing alone. The results of the nonlinear examples are in very good agreement with those obtained from the Fourier–Hermite method up to the time limit of validity of the latter method. However, the cost of computation with the third order ASD method is only one-tenth of that with the Fourier–Hermite method for similar overall accuracy.

REFERENCES

1. J. GAZDAG, *J. Computational Phys.* **13** (1973), 100–113.
2. J. GAZDAG, in "Proceedings of the 1973 Summer Computer Simulation Conference," Montreal July 17–19, 1973, pp. 40–45.
3. J. GAZDAG AND J. CANOSA, *J. Appl. Probability* **11** (1974), 445–457.
4. J. GAZDAG AND J. CANOSA, in "Proceedings of the Sixth Conference on Numerical Simulation of Plasmas," Berkeley, Calif., July 16–18, 1973, p. C8.
5. J. GAZDAG, in "Proc. Intern. Symp. on Computing Methods in Applied Sciences and Engineering," Versailles, France, December 17–21, 1973, Lecture Notes in Computer Science, Vol. 11 (G. Goos and J. Hartmanis, Eds.) Part 2, p. 37, Springer–Verlag, Berlin/New York.
6. J. CANOSA AND J. GAZDAG, The Korteweg–de Vries–Burgers Equation, Report No. G320-3321, IBM Scientific Center, Palo Alto, California, January 1974.
7. J. CANOSA, J. GAZDAG, F. E. FROMM, AND B. H. ARMSTRONG, *Phys. Fluids* **15** (1972), 2299.
8. J. CANOSA AND J. GAZDAG, *Phys. Fluids* **17** (1974), 2030.
9. T. P. ARMSTRONG, R. C. HARDING, G. KNORR, AND D. MONTGOMERY, in "Methods in Computational Physics," Vol. 9, pp. 30–84, Academic Press, New York, 1970.
10. I. B. BERNSTEIN, *Phys. Rev.* **109** (1958), 10.
11. G. BEKEFI, "Radiation Processes in Plasmas," p. 238, Wiley, New York, 1966.
12. S. J. GITOMER, *Phys. Fluids* **14** (1971), 2234.
13. J. GAZDAG, in "Proc. Fourth Conference on Numerical Simulation of Plasmas," Washington, D.C., Nov. 2–3, 1970, p. 665.
14. G. JOYCE AND G. KNORR, *Phys. Fluids* **15** (1972), 177.
15. J. CANOSA, J. GAZDAG, AND J. E. FROMM, *J. Computational Phys.* **15** (1974), 34.
16. J. NÜHRENBERG, *Z. Angew. Math. Phys.* **22** (1971), 1057.
17. G. KNORR, *J. Computational Phys.* **13** (1973), 165.
18. R. C. DAVIDSON, "Methods in Nonlinear Plasma Theory," Academic Press, New York, 1972.